FIRST STEPS OF A MILLIMETER-SCALE WALKING SILICON ROBOT

Daniel S. Contreras, Daniel S. Drew, and Kristofer S. J. Pister
University of California, Berkeley, CA, USA

ABSTRACT

This work presents the locomotion of a ground-based single-legged silicon robot. The robot measures 5mm x 6mm x 0.5mm and weighs 18mg. Fabricated in a silicon-on-insulator (SOI) process, the robot is based on electrostatic inchworm motors that drive a 2 degree-of-freedom (DOF) planar silicon linkage that acts as the leg. The leg sweeps out an area of approximately 500µm x 500µm off the edge of the chip. The chip is connected to power and control by long flexible wires which also act to support the robot upright. The robot exerts over 1.5x its weight in the vertical axis, enough to lift its body and push itself forward.

KEYWORDS

microrobotics, silicon-on-insulator, electrostatic, inchworm, motors, linkage

INTRODUCTION

Designers of millimeter-scale to centimeter-scale robots have explored a wide variety of actuators and mechanisms for the purpose of mobility. Piezoelectric muscle-like actuators in combination with flexures have been demonstrated to work for both air-based and ground-based centimeter-scale robots [1,2]. Shape memory alloy actuators have been used to drive a hand-assembled silicon linkage [3]. Millimeter-scale robots actuated via external electric and magnetic fields have been demonstrated [4-6]. Work has also shown a robot based on an electrostatic self-sustaining resonance mechanism [7]; this robot was even able to walk using its own on-board power source.

For autonomous microrobots, electrostatic actuators are appealing for their low power draw when compared to thermal and piezoelectric actuators and the scale invariant nature of electrostatic forces. A previous attempt at creating a fully autonomous millimeter-scale walking robot focused on designing a silicon linkage that could move out of the plane of the fabricated chip [8]. The robot carried its own on-board solar cells and drive circuit and was able to lift itself off the ground but it was unable to move forward.

Our robot is based on a similar approach, using electrostatic inchworm motors to drive a silicon linkage. However, rather than focusing on a complex process flow to achieve out-of-plane motion, the robot is designed with its actuators and linkage moving entirely in the plane of the fabricated chip. The leg sweeps out an area off the edge of the chip and the chip is oriented vertically after fabrication so that the leg can actuate on the ground. An image of the robot standing upright is shown in Fig. 1.

The single-legged robot shown in this work was developed as a test case for this method of vertical chip actuation. After demonstrating the success of this locomotion mechanism, the next step will be to implement this actuation scheme in a more biologically inspired multi-legged robot.

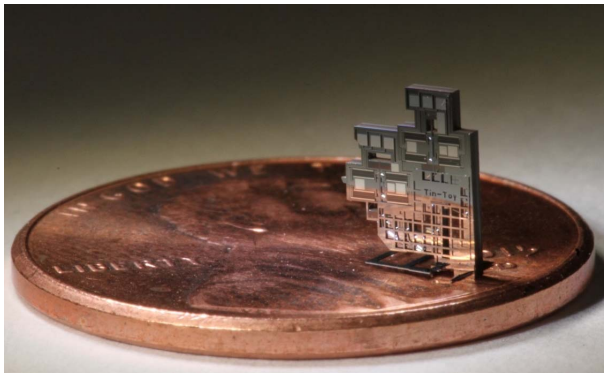

Figure 1: The robot standing upright on a US penny. The robot is able to stand upright using microassembled support feet in the main body and the leg

DESIGN AND FABRICATION

Electrostatic Inchworm Motors

Angled-arm electrostatic inchworm motors were first fabricated and tested in [9]; our motors were designed using the optimization scheme presented therein. The motors are made of a set of four identical gap closing actuator (GCA) arrays with angled arms attached to their ends. Two GCA arrays engage to impact the central shuttle and move the shuttle forward. Working in tandem with the other pair of GCA arrays, the actuators are able to produce over 500µm of displacement on the shuttle at over 1mN of output force. Long throw serpentine springs support the shuttle and allow for large displacements. Since the motors are unidirectional, the serpentine springs also reset the shuttle position once the motor reaches its end of travel.

Silicon Pin-Joints and Linkage Design

Single-mask SOI pin-joints were first investigated for applications in microrobotics in [10] and were further characterized in [11]. As compared to flexures, pin-joints provide a low-force, low-friction way to create linkages in silicon. These joints have a single rotational DOF and are unable to perform full revolutions since they are fabricated in a single layer of silicon. Because of this, and because we are limited to linear actuation from our chosen electrostatic actuators, more complex linkage designs are necessary for full circuit sweeps like those seen in simple macroscale 4-bar linkages with a single DOF rotary input.

The base leg design for our robot is a selective 4-bar linkage shown in Fig. 2. Two linear motors attach to the linkage as indicated. The linkage has 2 DOF and each DOF is actuated by a single motor at any given time while the other motor holds its attachment point and DOF anchored. In this way the linkage performs full circuit sweeps.

Additional links were included in the final design to

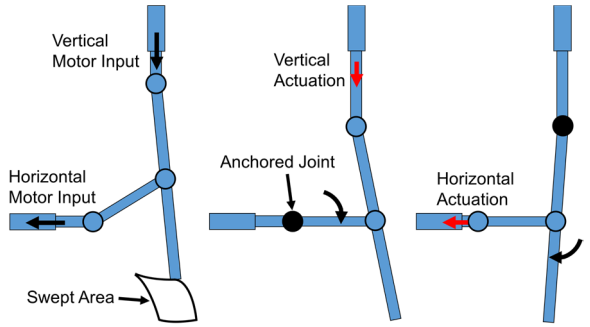

Figure 2: Diagram showing leg actuation. Motors are connected to the linkage as indicated to achieve the swept area shown. At any given time, a single motor operates the linkage while the other motor holds its attachment point anchored

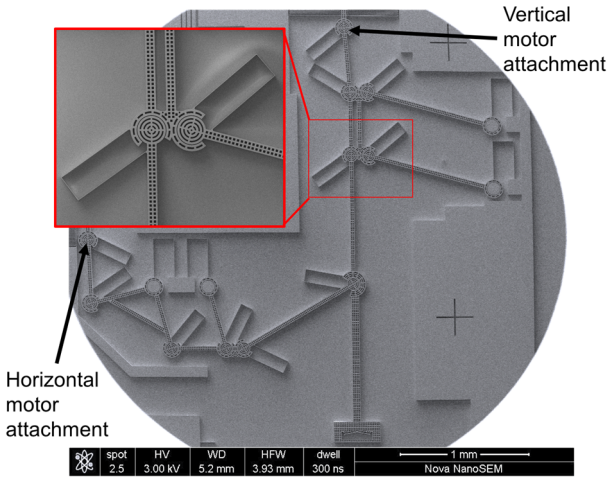

Figure 3: An SEM micrograph of the linkage showing the motor attachment points and a detail of the pin-joints used in the design

isolate the inchworm motor shuttle from the effects of any lateral forces and moments that might be transmitted from the leg as well as to orient the motors for compactness. The full leg is a 13-bar linkage with 17 joints. At any given time, the leg operates as an 8-bar linkage with 10 joints.

Fig. 3 shows a fabricated robot linkage SEM micrograph, highlighting the motor attachment points and a detail of a set of pin-joints. Fig. 4 shows a full robot with the motors and linkage highlighted.

Microassembled Support

The silicon pin-joints are sensitive to out-of-plane forces above 100µN. Higher forces are enough to pop the pin-joints out of plane. In order to mitigate this issue, a protective screen is glued on top of the linkage using silver epoxy. This screen is bonded well enough to hold the linkage in plane. An assembled robot with a screen glued onto the linkage is shown in Fig. 4.

Fabrication and Assembly

The robot is fabricated in a 2-mask SOI process. Wafers with a 40µm device layer, 2µm buried oxide, and 550µm substrate are used. Motors and the linkage are etched into the frontside device layer silicon using DRIE.

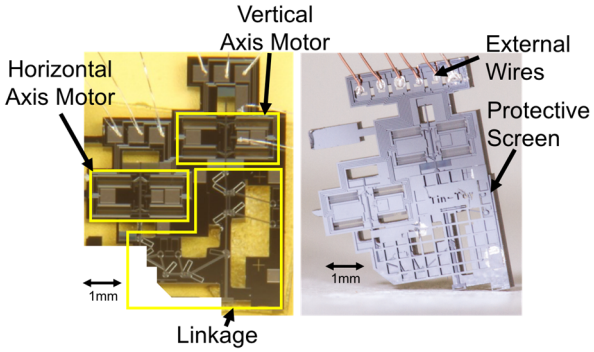

Figure 4: A fabricated robot wirebonded to a chip package. The motors and the linkage are highlighted (left) A tethered upright robot. Insulated 60µm copper wires are bonded to the motor drive pads using silver epoxy. The protective screen is glued over the linkage, also using silver epoxy (right)

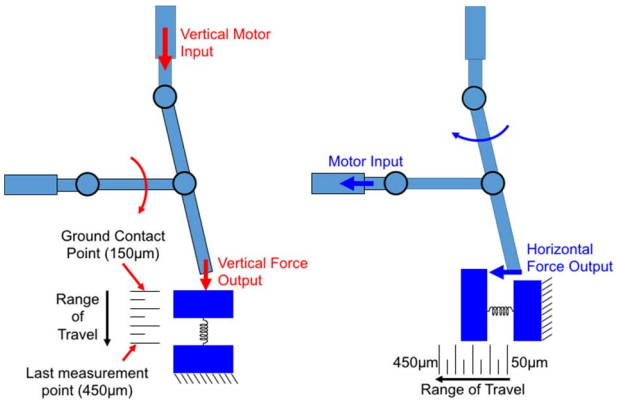

Figure 5: Setup for measuring the force output of the leg. The linkage pushes on a spring-based vernier gauge that is positioned with probe tips. Force is measured by reading the displacement on the vernier

A backside DRIE is used to reduce the robots mass and free the robot from the rest of the wafer. The linkage and motors are released from the buried oxide layer using a vapor-phase HF etch. The released robot chip is then assembled by hand for testing.

EXPERIMENTAL SETUP

Measuring Force Output

Force output of the motors and the linkage was measured using spring-based vernier gauges fabricated alongside the structures. Inchworm motors with springs attached to the shuttle were fabricated. The inchworm motors were driven until the springs stopped the shuttle. This displacement is read and taken as the maximum motor output force. The max force is taken for varying applied voltages.

For the linkage, a gauge on a flexible support assembly is moved with probe tips so that the linkage is able to push on the gauge at various positions. A diagram of the setup is shown in Fig. 5. The force output was measured at 50µm increments from the leg's rest position. The linkage has a sweep of approximately 500µm in either direction and force measurements were taken to within 50µm of the max

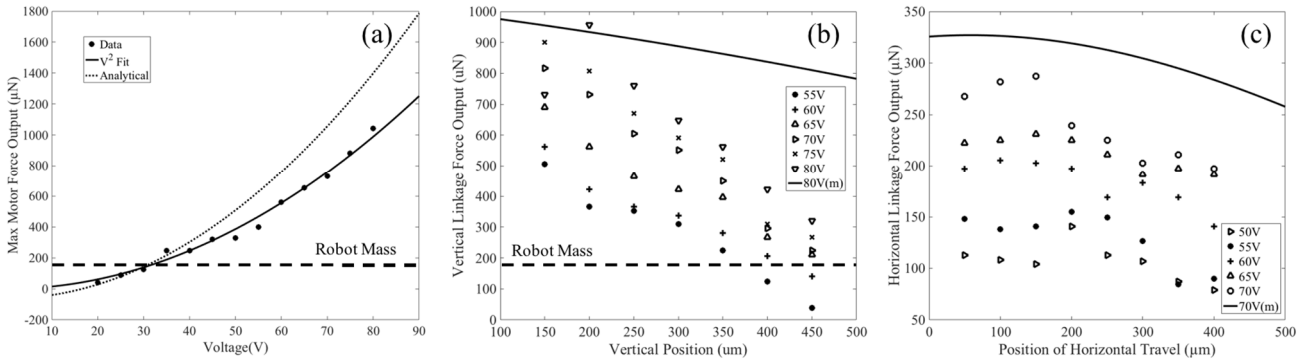

Figure 6: Force output of the motor and the linkage (a) The force output of the raw inchworm motor. The larger dashed line indicates the target robot mass of 20mg, the smaller dashed line is the calculated force output from the optimization scheme, and the solid line is a V^2 fit to the data. At 80V, the robot exerts over 1mN of force, enough to lift about 5x the robot's mass (b) The force output of the linkage in the vertical direction, the axis where the robot lifts itself. The solid line indicates the modeled linkage force output with losses from the spring support and mechanical disadvantage factored in (c) The force output of the linkage in the horizontal direction. Again, the solid line indicates modeled linkage force output taking losses into account

deflection. The leg pushes on the gauge until it stalls. This maximum displacement is read off the gauge and related to the output force by the spring constant of the gauge. All spring gauges are calibrated using comb drive resonators.

Demonstrating Walking

The robot was tethered to external power and control using flexible insulated 60μm copper wires. Fig. 4 shows a robot with wires attached standing upright. The robot is suspended by its wires from a vertical positioning stage. The stage is lowered onto a scale until the scale reads the robot's mass of 18mg. The wire suspension is able to hold the robot upright without need for support during its walk cycle.

RESULTS

Force Output

The force output of the inchworm motor is shown in Fig. 6(a). The motor exerts over 1mN of force at 80V. This is about 5x the amount of force necessary to lift the robot's measured mass of approximately 18mg. There is a discrepancy between the expected force output and the measured force output. At 80V the measured force is about 75% of the calculated force output from the optimization scheme used. This could be the result of variations in the gap distance at which the motors engage the shuttle, caused by issues in lithography or by movement of the motor shuttle towards/away from the angled arm pawls due to unaccounted for moments.

Force output from the linkage in the vertical and horizontal axes is given in Fig. 6(b) and Fig. 6(c) respectively. In the vertical axis, we see a drop off in force output as the leg extends. The loss is attributed to extension of the serpentine support springs, rotation of the pin-joint support springs, and inherent mechanical disadvantage in the linkage.

The solid line indicates the modeled force output factoring force losses from the support springs and the mechanical disadvantage of the linkage. There is a discrepancy between the modeled force output and the measured force output. Part of this may be attributed to frictional losses in the linkage joints and between the linkage and the substrate. There was also noticeable slipping between the foot of the robot and the contact point of the vernier gauge during some measurements.

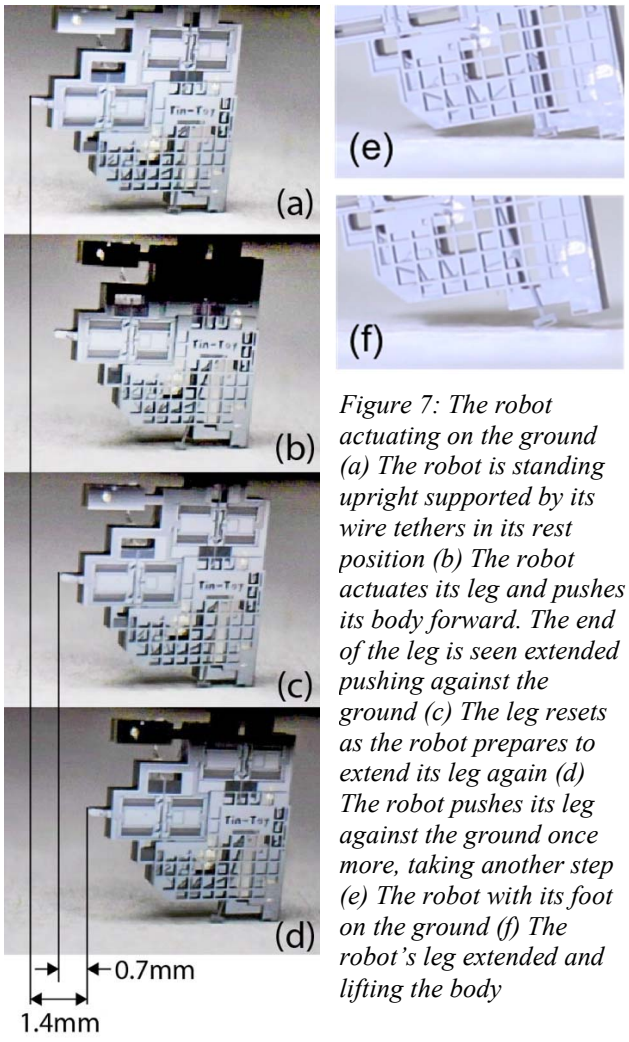

Figure 7: The robot actuating on the ground (a) The robot is standing upright supported by its wire tethers in its rest position (b) The robot actuates its leg and pushes its body forward. The end of the leg is seen extended pushing against the ground (c) The leg resets as the robot prepares to extend its leg again (d) The robot pushes its leg against the ground once more, taking another step (e) The robot with its foot on the ground (f) The robot's leg extended and lifting the body

Tethered Walking

Fig. 7 shows the robot actuating on the ground while tethered. The robot was able to pick itself up with its foot actuating at 80V. Fig. 7(a)-(d) show a sequence of the robot walking. Rather than lifting its body and taking a stride during its walk cycle, the leg would slip on the ground behind the robot and push its leg on the ground. The robot was able to push itself forward in this manner, against its tethers and mass.

Actuating the motor GCA arrays at 500Hz, the walking speed was 0.7mm/s, about 0.15 body lengths per second. This frequency corresponds to an unloaded inchworm shuttle speed of about 2mm/s. At this speed, a full step would take about 0.5s giving a theoretical walking speed of 1mm/s. The lower measured walking speed could be attributed to the robot not being able to complete its full stride due to force loss. Ongoing work on the dynamics of the motors has demonstrated speeds up to 30mm/s, so the robot can potentially move much faster.

Fig.7 (e)-(f) shows the robot lifting its body. The robot is positioned such that the foot of the suspended robot is in contact with the ground. The leg extends and the robot is able to pick itself up. Occasionally the voltage would have to be raised to 90V for the robot to actuate. This was assumed to be caused by extra friction from the linkage on the protective screen.

Power Draw

Capacitance between the actuating fingers and between the drive fingers and the substrate was measured using an AD7746 evaluation board. When closed, the fingers measured 2.1pF. The capacitance to the substrate was about 10.3pF. Being driven at 500Hz, the total power draw for the robot is about 80μW. The solar cells presented in [8] were able to generate 100μW of power and weighed 2.3mg. Using these solar cells, with proper mass reduction of the robot's substrate, our robot would be able to carry this power source.

CONCLUSION

Using a set of electrostatic inchworm motors to drive a 2 DOF silicon linkage, we have demonstrated a single-legged walking millimeter-scale robot. The inchworm motor and linkage are all fabricated to move in the plane of the chip. The robot chip is flipped vertically to actuate on the ground. In this way, we have forgone complex out-of-plane linkage design in favor of post-processing assembly and support design.

Moving forward, many aspects of this design have yet to be optimized. The 550μm substrate serves merely as a skeleton for the robot and can be greatly reduced to lower the robot's mass and increase the payload capacity. The design behind the tethering can also be improved. Additionally, the single legged walking design is not stable for walking without tether supports. Future work will focus on multi-legged statically stable robot designs. These robots will use multichip assembly to add support and routing to chips with multiple legs.

This robot serves as the initial test case for a new design platform for silicon microrobots using low power electrostatic inchworm motors fabricated alongside silicon linkages, combined with lightweight energy sources and computation. The goal for this platform is two-fold; to develop robots with a tenable path towards autonomy as well as to create modular components fabricated in a reproducible process that can be widely disseminated.

ACKNOWLEDGMENTS

All devices were fabricated in the UC Berkeley Marvell Nanofabrication Laboratory. Thanks to Joseph Greenspun for help with taking SEM micrographs.

REFERENCES

[1] R. Wood, "The First Takeoff of a Biologically Inspired At-Scale Robotic Insect", in *IEEE Trans. Robotics,* vol. 24, no. 2, pp. 341-347, 2008.

[2] A. T. Baisch, O. Ozcan, B. Goldberg, D. Ithier, and R. J. Wood, "High Speed Locomotion for a Quadrupedal Microrobot," in *Int. J. of Robotics Research*, vol. 33, no. 8, pp. 1063–1082, 2014.

[3] K. Saito, K. Iwata, Y. Ishihara, K. Sugita, M. Takato, and F. Uchikoba, "Miniaturized Rotary Actuators Using Shape Memory Alloy for Insect-Type MEMS Microrobot," in *Micromachines*, vol. 7, no. 4, p. 58, 2016.

[4] D. Vogtmann, R. S. Pierre, and S. Bergbreiter, "A 25 mg Magnetically Actuated Microrobot Walking at > 5 Body Lengths/Sec," in *IEEE Int. Conf. on MEMS*, Las Vegas, Nevada, USA, 2017. pp. 179–182.

[5] R. Pelrine *et al.*, "Diamagnetically Levitated Robots: An Approach to Massively Parallel Robotic Systems with Unusual Motion Properties," in *Int. Conf. on Robotics and Automation,* 2012, pp. 739–744.

[6] B. R. Donald, C. G. Levey, C. D. McGray, I. Paprotny, and D. Rus, "An Untethered, Electrostatic, Globally Controllable MEMS Micro-Robot," in *J. of Microelectromechanical Systems*, vol. 15, no. 1, pp. 1–15, 2006.

[7] M. Qi, Y. Zhu, Z. Liu, X. Zhang, X. Yan, and L. Lin, "A Fast-Moving Electrostatic Crawling Insect," in *IEEE Int. Conf. on MEMS*, Las Vegas, Nevada, USA, 2017. pp. 761–764.

[8] S. Hollar, A. Flynn, C. Bellew, and K. S. J. Pister, "Solar Powered 10 mg Silicon Robot," in *IEEE Int. Conf. on MEMS*, Kyoto, Japan, 2003, pp. 706–711.

[9] I. Penskiy and S. Bergbreiter, "Optimized Electrostatic Inchworm Motors Using a Flexible Driving Arm," in *J. of Micromechanics and Microengineering*, vol. 23, no. 1, p. 15018, Jan. 2013.

[10] A. M. Mehta and K. S. Pister, "Flexure-Based Two Degree-of-Freedom Legs for Walking Microrobots," in *ASME Int. Mechanical Engineering Congress and Exposition*, 2006, pp. 441–450.

[11] D. S. Contreras and K. S. J. Pister, "Durability of Silicon Pin-Joints for Microrobotics," in *Int. Conf. on Manipulation, Automation and Robotics at Small Scales*, Paris, France, 2016.

CONTACT

*D.S. Contreras; dscontreras@berkeley.edu